



Contents lists available at ScienceDirect

Planetary and Space Science

journal homepage: www.elsevier.com/locate/pss

Regions of interest (ROI) for future exploration missions to the lunar South Pole

J. Flahaut^{a,*}, J. Carpenter^b, J.-P. Williams^c, M. Anand^d, I.A. Crawford^e, W. van Westrenen^f, E. Fűri^a, L. Xiao^g, S. Zhao^g

^a Centre de Recherches Pétrographiques et Géochimiques (CRPG), CNRS/ Université de Lorraine, 15 Rue Notre-Dame des Pauvres, 54500, Vandœuvre-lès-Nancy, France

^b ESA-ESTEC, Noordwijk, the Netherlands

^c Department of Earth, Planetary, and Space Sciences, University of California, USA

^d School of Physical Sciences, The Open University, Milton Keynes, UK

^e Department of Earth and Planetary Sciences, Birkbeck College, University of London, London, UK

^f Department of Earth Sciences, Faculty of Science, Vrije Universiteit (VU), Amsterdam, the Netherlands

^g Planetary Science Institute, China University of Geosciences, Wuhan, 430074, China

ARTICLE INFO

Keywords:

Lunar poles
Volatiles
ISRU
Water ice
Landing sites
GIS

ABSTRACT

The last decades have been marked by increasing evidence for the presence of near-surface volatiles at the lunar poles. Enhancement in hydrogen near both poles, UV and VNIR albedo anomalies, high CPR in remotely sensed radar data have all been tentatively interpreted as evidence for surface and/or subsurface water ice. Lunar water ice and other potential cold-trapped volatiles are targets of interest both as scientific repositories for understanding the evolution of the Solar System and for exploration purposes. Determining the exact nature, extent and origin of the volatile species at or near the surface in the lunar polar regions however requires *in situ* measurements via lander or rover missions. A number of upcoming missions will address these issues by obtaining *in situ* data or by returning samples from the lunar surface or shallow subsurface. These all rely on the selection of optimal landing sites. The present paper discusses potential regions of interest (ROI) for combined volatile and geologic investigations in the vicinity of the lunar South Pole. We identified eleven regions of interest (including a broad area of interest (>200 km × 200 km) at the South Pole, together with smaller regions located near Cabeus, Amundsen, Ibn Bajja, Wiechert J and Idel'son craters), with enhanced near-surface hydrogen concentration ($H > 100$ ppm by weight) and where water ice is expected to be stable at the surface, considering the present-day surface thermal regime. Identifying more specific landing sites for individual missions is critically dependent on the mission's goals and capabilities. We present detailed case studies of landing site analyses based on the mission scenario and requirements of the upcoming Luna-25 and Luna-27 landers and Lunar Prospecting Rover case study. Suitable sites with promising science outcomes were found for both lander and rover scenarios. However, the rough topography and limited illumination conditions near the South Pole reduce the number of possible landing sites, especially for solar-powered missions. It is therefore expected that limited Sun and Earth visibility at latitudes $>80^\circ$ will impose very stringent constraints on the design and duration of future polar missions.

1. Introduction

For over half a century, scientists have been debating the existence of water ice and other cold-trapped volatiles at the lunar poles (e.g., Watson et al., 1961; Arnold, 1979; Ingersoll and Murray, 1992; Feldman et al., 2001; Anand, 2010; Paige et al., 2010; Hayne et al., 2015; Li et al., 2018). Because of the low inclination of the Moon's rotational axis, illumination conditions at the poles are extreme, and regions of permanent shadow

exist at latitudes $>65^\circ$. Areas that never receive direct sunlight (referred to as permanently shadowed regions, PSRs) are invariably cold (~ 40 K) and considered as possible reservoirs for ice sequestration (Ingersoll and Murray 1992; Paige et al., 2010). Multiple evidence from recent orbiter missions seem to confirm the presence of water ice and other volatiles inside, but also outside of PSRs, drawing more attention to the lunar poles these last years (e.g., Colaprete et al., 2010; Hayne et al., 2015; Li et al., 2018). Water ice and other volatiles on the Moon are fundamental

* Corresponding author.

E-mail address: jessica.flahaut@univ-lorraine.fr (J. Flahaut).

<https://doi.org/10.1016/j.pss.2019.104750>

Received 13 May 2019; Received in revised form 13 September 2019; Accepted 17 September 2019

Available online xxx

0032-0633/© 2019 Elsevier Ltd. All rights reserved.

tracers of dynamical material exchange among different regions of the Solar System (e.g., Lin and van Westrenen, 2019), but are also key to understanding the Moon's origin and evolution (e.g., Anand et al., 2014; Lin et al., 2017). In addition, cold-trapped volatiles might represent valuable resources to support future lunar infrastructures and space exploration in general (e.g. Anand et al., 2012; Crawford et al., 2012).

A number of studies have been initiated in the past years, making use of the wealth of available remote sensing datasets, to highlight potential regions of interest for future lunar missions aimed at investigating the cold-trapped polar volatiles, with a stronger focus on the South Pole. Situated within the outer portion of the South-Pole Aitken (SPA) basin, the South Pole offers a unique opportunity to determine the age and the structure of this basin, which is the largest (~2600 km diameter) and oldest known impact structure in the Solar System (e.g., Wilhelms et al., 1979; Spudis et al., 1994). Because of this additional scientific benefit of outstanding value, the South Pole tends to be favored compared to the North Pole for upcoming missions, and is the focus of this paper.

Lemelin et al. (2014) used a multi-parameter analysis to select optimal landing sites for returning volatile-rich samples from the poles. The authors searched for suitable landing sites where concept 4 of the NRC report (2007) "The lunar poles are special environments that may bear witness to the volatile flux over the latter part of solar system history" could be best addressed. They identified the regions with the best chances of containing accessible volatiles as those (1) in permanently shaded regions, (2) with enhanced hydrogen abundances (greater than 150 ppm), (3) maximum annual temperature between 0 and 54 K, (4) minimum annual temperature between 0 and 54 K, (5) average annual temperature between 0 and 130 K, and (6) shallow slopes (shallower than 25° for rover mobility constraints). They found two such sites in the south polar region (Shoemaker and Faustini craters), and two in the north polar region (Peary crater and a region between Hermite and Rozhdestvenskiy W craters). They relaxed the constraints, allowing one of the six criteria to be suboptimal, and identified five additional sites in the south polar region (Haworth, De Gerlache, and Cabeus craters as well as a region between Shoemaker and Faustini craters and the northern portion of Amundsen crater) and three additional sites in the north polar region (Lenard, Hermite and Rozhdestvenskiy W craters). Given that these sites are all located within PSRs, they might however be challenging to access with a solar-powered spacecraft.

The same year, a LEAG team (the VSAT – Volatile Specific Action Team) was tasked by NASA to make landing site recommendations for future missions. Largely based on the Lemelin et al. (2014) study, but varying thresholds and adding constraints on the Sun and Earth visibility, the LEAG team proposed regions of interest (ROI) near Cabeus and Shoemaker in the South Pole region. This selection was largely based on the imposed requirement that H abundance, as estimated from the Lunar Prospector Neutron Spectrometer (LPNS) data, had to be above 150 ppm, among other criteria (annual surface temperature >110K, modest slopes <10°, proximity of PSRs (<1 km)) (LEAG VSAT, 2015).

In 2015, an ESA team published a response to the LEAG report (ESA TT ELPM, 2015). The European recommendations in terms of orbiter and lander measurement findings were similar to those of the LEAG report. The ESA study however considered the possibility of combining volatile studies with additional scientific (geologic) investigations. The team proposed to work with an enlarged set of parameters, that account for potential additional science benefits (and hence consider the possibility to fill more science concepts of the NRC report), to define regions of interest near the poles. In particular, relaxing the H abundance threshold to 125 ppm and the need to be within 1 km of a PSRs (which mostly applies to a rover-scenario) resulted in a more extended area available for exploration (ESA TT ELPM, 2015; Flahaut et al., 2016a, b).

The present paper describes regions of interest that address multiple science questions such as the nature and distribution of polar volatiles (NRC concept 4), but also the potential to investigate the lunar chronology (NRC science concept 1), lunar interior (NRC concept 2), and the lunar crust diversity (NRC concept 3) (NRC, 2007). Section 2 summarizes

the start-of-the art knowledge of the South Pole environment that addresses some challenges anticipated for future lunar missions. The datasets and methods used to define ROIs are listed in Section 3. Given that finding a candidate landing site is very specific to a mission's objectives and design, broad areas of interest are presented in section 4. We then present three detailed landing site analysis case studies based on the characteristics of some planned (or studied) missions to the South Pole: Luna-25, Luna-27 and ESA's Lunar Prospecting Rover (LPR) concept (Section 5). Example traverses along the Shoemaker-Faustini ridge are presented for the rover case study.

2. The South Pole environment

The South Pole region is marked by a rough topography, owing to its location on the SPA rim and superimposed impacts (e.g., Wilhelms et al. 1979; Spudis et al., 2008). Elevation ranges from about –8000 to +8000 m with slopes as steep as 80° (Fig. 1a and b). Because of this rough topography and the Moon's small axial inclination (1.54°), illumination conditions at the South Pole are extreme (e.g., Bussey et al., 1999, 2010; Noda et al., 2008; Mazarico et al., 2011). Most polar locations receive sunlight for less than 50% of the time, as illustrated by low illumination fraction values (<0.5) on Fig. 1c. Lunar Orbiter Laser Altimeter (LOLA) based simulations over long time-periods (several 18.6-year lunar precession cycles) at 240 m/pixel and down to ~75° latitude revealed that PSRs extend beyond the expected PSR crater floors and represent a total area exceeding 16,000 km² near the South Pole (e.g., Bussey et al., 2003; Zuber and Smith, 1997; Margot et al., 1999; McGovern et al., 2013; Mazarico et al., 2011, their Fig. 8). Still, areas of limited extent that experience nearly-persistent illumination (over 80% of the day on average) were identified near the rims of Shackleton and De Gerlache craters and the connecting ridge in between, but also on the rim of Nobile crater and on the crest of the Malapert Massif (e.g., Fig. 12 of Mazarico et al., 2011; Fig. S1). For most of these locations, a small height gain of a solar panel (2–10 m) can significantly improve illumination conditions, providing a near-continuous source of power, and making them interesting targets for future exploration missions (e.g., Mazarico et al., 2011; De Rosa et al., 2012; McGovern et al., 2013; Speyerer and Robinson, 2013; Gläser et al., 2014, 2018). The characteristics of these regions are briefly discussed in the next sections, and presented in Fig. S2.

With average annual surface temperatures as low as 38 K near the lunar South Pole; PSRs are cold enough for cold-trapped volatiles, including water ice, to be present (Zhang and Paige, 2009; Paige et al., 2010, Fig. 1g). Data acquired by various remote sensing instruments in orbit around the Moon suggest that water frost is present at the surface or subsurface in some PSRs, and beyond. Surface frost could explain anomalies in Lyman Alpha Mapping Project (LAMP) and LOLA 1064 nm surface albedo, which are rather well correlated, and suggest the presence of 1–10% water ice (Hayne et al., 2015; Lucey et al., 2014; Fisher et al., 2017, Fig. 2a). Many of these locations also exhibit diagnostic near-infrared absorption features of water ice in reflectance spectra acquired by the Moon Mineralogy Mapper (M³) instrument (Li et al., 2018). The LPNS and Lunar Energetic Neutron Detector (LEND) have measured enhanced Hydrogen concentrations around the South Pole, with estimates of 0.3–0.5 wt% Water-Equivalent Hydrogen (WEH) within the uppermost meter of the surface in PSRs (e.g., Feldman et al., 2001; Mitrofanov et al., 2012a; Sanin et al., 2016; Lawrence, 2017, Fig. 1e and f). Spatially deconvolved neutron data for 12 PSRs yield WEH values in the range of 0.2–~3 wt%, with an average of 1.4 wt% (Teodoro et al., 2010). Both Deep Impact and M³ Visible Near Infra-Red (VNIR) hyperspectral data show latitudinal variations in the strength of the 3 μm OH/H₂O absorption band (Pieters et al., 2009; Sunshine et al., 2009). However, the nature and origin of the hydrogen-host phase(s) are uncertain. Potential sources of H include comet and asteroid impacts, solar wind implantation, and outgassing from the lunar interior (e.g., Anand et al., 2014); these different contributions could potentially be distinguished based on hydrogen isotope (D/H) ratio measurements (e.g., Fürti

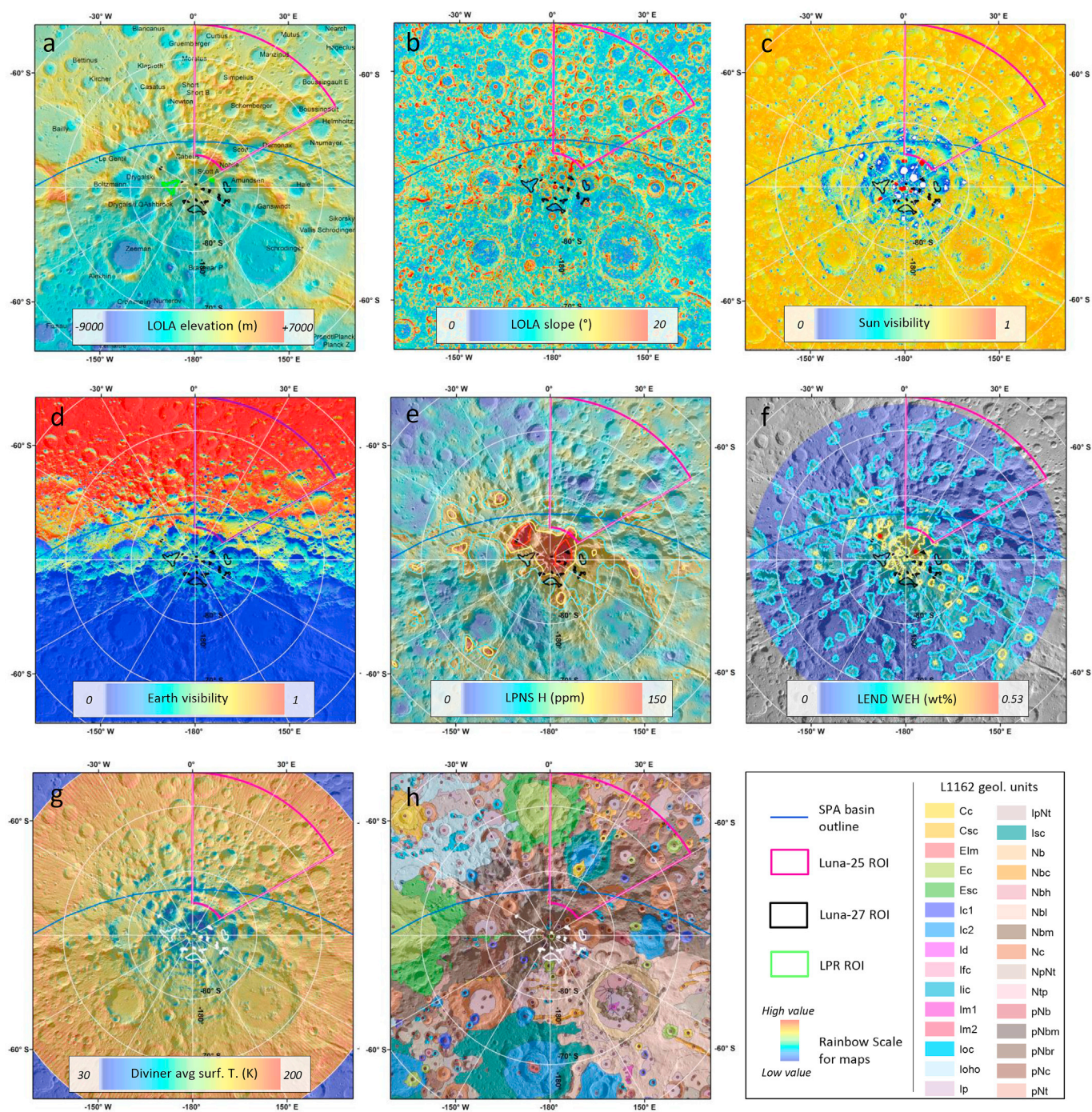


Fig. 1. Maps of the lunar South Pole, from latitudes 65–90° S (polar stereographic projection). A) LOLA DEM overlain on the LROC WAC mosaic. The blue line indicates the outline of the SPA impact basin. The magenta outline indicates the region investigated for Luna-25 landing sites. Sites that are recommended for the Luna-27 (black and green) and the LPR (green) case studies are also shown (see next sections). b) LOLA-derived slope map at 120 m/pixel. c) Average visibility of the Sun as seen from a given point on the Moon. Visibility varies between 0, when the sun is not visible, and 1, when any part of it is. Red dots indicate the highly illuminated sites discussed in Mazarico et al. (2011) (Also see Fig. S1). d) Average visibility of Earth as seen from a given point on the Moon. Visibility varies between 0, when Earth is not visible, and 1, when any part of it is. e) LPNS H abundance map. Contours at 100 ppm (blue), 125 ppm (yellow) and 150 ppm (red) are indicated to highlight enhanced signatures. f) LEND water-equivalent hydrogen map. Contours at 0.1 wt% (blue), 0.2 wt% (yellow) and 0.5 wt% (red) are indicated to highlight enhanced signatures. g) Diviner average temperature map. h) Excerpt of the USGS geological map L-1162. The reader is to refer to the text for data resolution and sources. (For interpretation of the references to color in this figure legend, the reader is referred to the Web version of this article.)

and Marty, 2015), either through *in situ* volatile studies or laboratory analyses of returned samples.

Spectral analyses of the Lunar Crater Observation and Sensing Satellite (LCROSS) impact plume in Cabeus crater provide tantalizing clues

to the nature of some polar volatiles. In addition to $\sim 5.6 \pm 2.9\%$ water ice in the regolith (by mass), a number of other volatile compounds were observed, including light hydrocarbons, sulfur-bearing species, and carbon dioxide (Colaprete et al., 2010; Gladstone et al., 2010). An

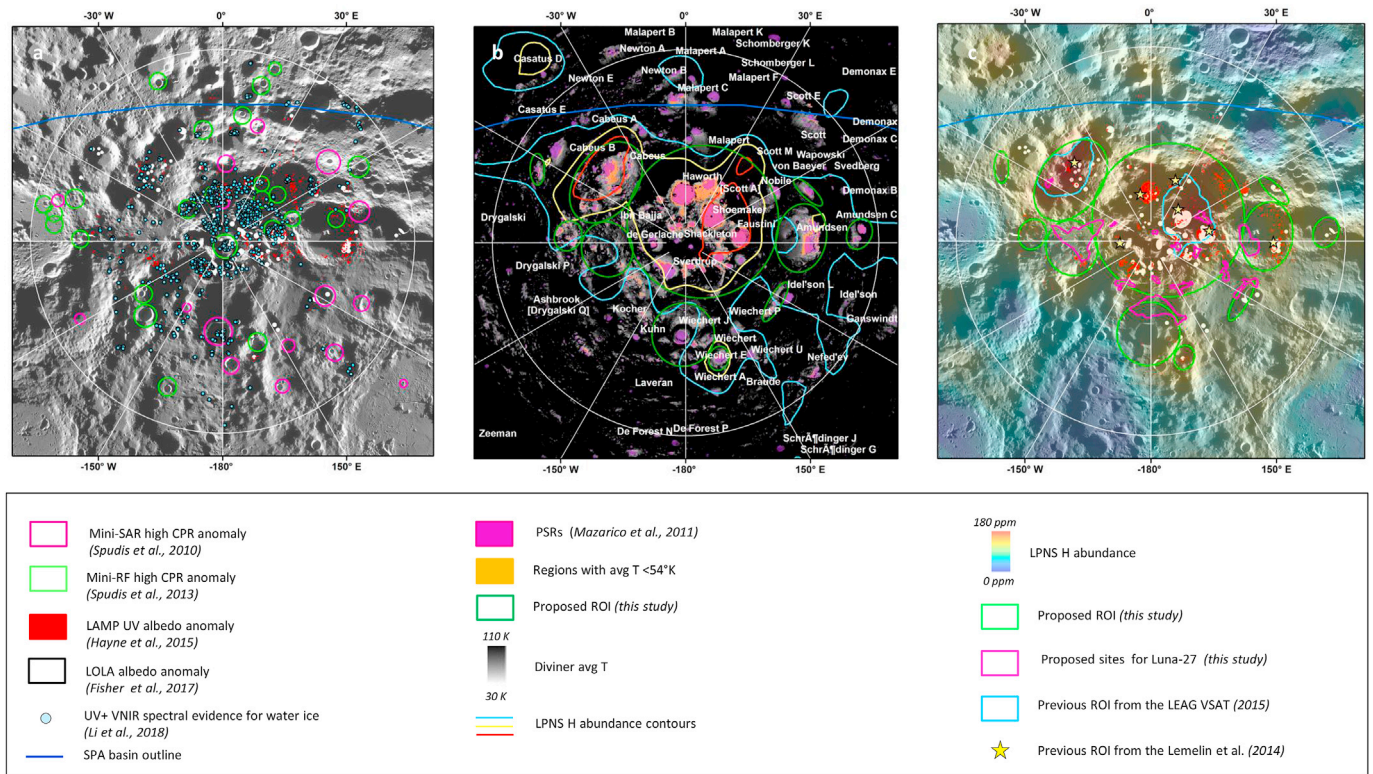


Fig. 2. Maps of the lunar South Pole, from latitudes 80–90° S (polar stereographic projection). A) LAMP UV albedo anomalies, LOLA anomalously bright pixels (which might be indicative of surface frost) as well as mini-SAR and mini-RF high CPR anomalies (which might be indicative of water ice at shallow depths, or freshly exposed material) and M³ VNIR ice detections are overlain on the LROC WAC mosaic. The blue line indicates the outline of the SPA impact basin. b) Proposed ROIs (green circles) are overlain on a map where Diviner average temperature > 110K and slope values > 20° were blackened. These ROIs encompass regions of enhanced H abundance, PSRs and regions with average T < 54K (where CO₂ ice should be stable at the surface). c) Proposed ROIs are compared with previous studies; background is a LPNS H abundance map. (For interpretation of the references to color in this figure legend, the reader is referred to the Web version of this article.)

opposition effect was also observed in the LRO mini-RF and Arecibo datasets on the floor of Cabeus and interpreted as evidence for the presence of water ice near the surface (Patterson et al., 2017). A same-sense polarization enhancement within the South Pole PSRs with the Clementine bi-static experiment was tentatively interpreted as showing the presence of low-loss volume scatterers, such as water ice (Nozette et al., 1996, 2001). High CPR acquired by the Chandrayaan-1 mini-SAR and the LRO mini-RF are well-correlated with PSRs and might also indicate the presence of discontinuous ice blocks at shallow depths (Spudis et al., 2010b, 2013, 2016, Fig. 2a). These observations, however, are not collocated with the predictions of ice stability at both the surface and depth made from Diviner’s present-day thermal infrared observations (e.g., Siegler et al., 2015, Fig. 2b). Altogether, current observations point to the existence of water ice, and possibly other cold-trapped volatiles (such as carbon monoxide, mercury, and sodium detected in the LCROSS plume, or ‘Super-volatiles’ – those with vapor pressures much higher than that of water – such as CO₂, CO, CH₄, NH₃, CH₃OH, and H₂S, which may be present as predicted by the temperature range), distributed heterogeneously at varying locations and depths in the polar regolith (e.g., Gladstone et al., 2010; Zhang and Paige, 2009; Hayne et al., 2019).

3. Remote sensing datasets

A wealth of remote sensing data has been collected in recent decades, providing crucial information pertaining to the existence of cold-trapped volatiles on the Moon. In the present paper, we collected a number of global data products that were gathered into a Geographic Information System (GIS), using ESRI ArcGIS software, for combined analyses.

3.1. These datasets include

- Lunar Reconnaissance Orbiter Camera (LROC) data; especially the Wide Angle Camera (WAC) global mosaic at 100m/pixel, and the Narrow Angle Camera (NAC) polar mosaics at ~1 m/pixel (Robinson et al., 2010),
- LOLA digital elevation models available at various spatial resolutions (from 10 m/pixel to 120 m/pixel) and derived slope maps (Smith et al., 2017),
- LOLA-based Sun and Earth visibility obtained from time averaging of computational modeling results performed every hour over ~18.6 years, and available at a resolution of 240 m/pixel (Mazarico et al., 2011). The average visibility is a fraction of time, equal to 0 when the Sun/Earth is not visible, and 1, when any part of it is. Illumination values used in this study indicate the fraction of time the Sun is visible from a given location.
- LOLA-based PSRs maps (Mazarico et al., 2011),
- LOLA albedo map at 1064 nm, at 1 km/pixel (Lucy et al., 2014; Lemelin et al., 2016) and anomalously bright pixels map (Fisher et al., 2017),
- Diviner Lunar Radiometer Experiment average, minimum, and maximum bolometric brightness temperature maps, as well as predicted ice depth stability at 240 m/pixel (Paige et al., 2010; Williams et al., 2017),
- LPNS Hydrogen abundance maps at ~15 km/pixel (Elphic et al., 2007; Feldman et al., 2001),
- LEND WEH map at ~2 km/pixel (Mitrofanov et al., 2012a),
- LAMP UV and off/on band albedo ratio at 240 m/pixel (Gladstone et al., 2012; Hayne et al., 2015),

- Mini Synthetic Aperture Radar (mini-SAR) Circular Polarization Ratio (CPR) map at ~ 75 m/pixel (Spudis et al., 2009, 2010a, 2016),
- Miniature radio frequency (Mini-RF) Circular Polarization Ratio (CPR) map from Spudis et al. (2013),
- USGS geological map L-1162 (Fortezzo and Hare 2013, renovation of the Wilhelms et al. (1979) map),
- Clementine UVVIS color ratio mineral map (e.g., Lucey et al., 2000; Heather and Dunkin, 2002), used at latitudes $< 80^\circ$. This RGB composite uses the 750/415 nm ratio for the red-channel brightness, the 415/750 nm ratio for the blue channel, and the 750/1000 nm ratio for the green channel. Color ratios allow identifying variations in mineralogical composition and/or terrain maturity.
- The Robbins (2018) impact crater database.

All data were downloaded from the Planetary Data System or instruments' websites and added to ArcGIS in a polar stereographic projection.

4. A global survey of potential ROIs in the vicinity of the South Pole

As stated above, different datasets indicative of the presence of water ice do not correlate perfectly in terms of spatial distribution (Fig. 2a and b). We identified 11 broad ROIs for future investigations by combining these datasets, using the following criteria:

- Diviner average temperature < 110 K (e.g., water ice is currently stable at the surface)
- Slope $< 20^\circ$ (Safe for landing and roving)
- Enhanced H signatures (> 100 ppm by weight, derived from LPNS data) (Ice should be present close to the surface).

These 11 ROIs include a broad region around the South Pole (comprising Shackleton, De Gerlache, Shoemaker, Faustini, Haworth, Nobile, Sverdrup craters) as well as smaller areas around Cabeus, Amundsen northern half, Amundsen C, Idel'son, Wiechert E, Wiechert J, and Ibn Bajja craters (see green circles on Fig. 2b and c). These regions show evidence for surface water ice based on either LAMP, LOLA or M³ datasets (e.g., Li et al., 2018, Fig. 2). Eight of these ROIs are located on the lunar nearside, and they are all located within the SPA basin. Thus, all the proposed ROIs offer the possibility to study both volatiles and SPA geology (see section 6.2). In addition, these ROIs cover various geological units, from pre-Nectarian (> 3.9 Ga) to Erastosthenian in age (from 3.2 to 1.1 Ga, De Gerlache, Wiechert J. for instance) and include one complex crater central peak (Amundsen), which might have excavated material from depths down to 16 km (using the depth of melting equation of Cintala and Grieve, 1998, in which the maximum depth of melting corresponds to the minimum depth of origin of central peak material). Three of the proposed ROIs encompass previously proposed sites and cover a wider area (Fig. 2c), as we allowed lower hydrogen abundance values than Lemelin et al. (2014) and LEAG VSAT (2015). Eight of the proposed ROIs are new and rely on the availability of data analyses published since the previous ROI definitions such as those based on LOLA (Fisher et al., 2017), LAMP (Hayne et al., 2015) and M³ (Li et al., 2018) reflectance. ROI are not prioritized in this study, as the final choice will be strongly mission dependent. Not all of the proposed ROIs offer good Sun or Earth visibility; as illumination is expected to be a limiting factor for any landing site at the South Pole, this aspect will be considered in the mission-specific case studies discussed below. Illumination is a key power source for most proposed missions, but, as shown in Fig. 1, it is anti-correlated with the average surface temperature measured by Diviner. All areas of average illumination $> 25\%$ around the South Pole are locations where water ice is not expected to be stable at the surface according to Diviner thermal models (Paige et al., 2010). Water ice is however predicted to be stable near the surface (< 1 m depth) at some of these locations, especially those surrounding massive PSRs (Paige et al.,

2010, Fig. 1). Restricted areas of average illumination $> 80\%$ were identified (Mazarico et al., 2011), however they should not bear water ice within the first meter of the surface (with the exception of a few pixels) and are poor candidates for volatile investigations (Figs. S1 and S2).

5. Selected case studies

Eleven broad ROIs, which appear suitable for landing and science investigations of polar volatiles, were identified in the previous section. However, identifying specific landing sites for individual missions is critically dependent on the mission's goals and capabilities. We present hereafter some examples of landing site analysis for mission scenarios currently under consideration. It should be noted however that the findings are relevant to a broad array of mission scenarios, including human missions to the lunar polar regions, for which constraints related to the environment and driving objectives are likely to be comparable to robotic missions. All the polar landing sites that will be proposed hereafter encompass the eleven broad ROI from this study (Fig. 2c).

5.1. The Luna-25 mission

Luna-Glob, or Luna-25, is an upcoming Russian lander mission, which aims to study the composition and physical properties of the regolith and surface volatiles in the vicinity of the lunar South Pole (e.g., Mitrofanov et al., 2012b). The Luna-25 lander will be equipped with a suite of instruments for *in situ* analyses, including a neutron and gamma-ray spectrometer, a laser mass spectrometer, an IR spectrometer, and several TV cameras (<http://www.iki.rssi.ru/eng/moon.htm>). Due to engineering constraints, it was previously formulated that potential landing sites for Luna-25 must meet the following criteria (Ivanov et al., 2015, 2017; Mitrofanov et al., 2016):

- The latitude and longitude of the landing site must be between 65 and 85°S and 0–60°E (Magenta outline on Fig. 1);
- The landing ellipse dimensions must be 15 km \times 30 km (elongated in longitudinal direction);
- Surface slopes within the landing ellipse must not be greater than 7° on a 2.5 m scale;
- The mean illumination within the landing area must be maximal;
- Earth visibility (for radio communication) within the landing area must be maximal;
- The hydrogen abundance as estimated from orbit must be maximal.

Constraints on illumination exclude higher latitude terrains and PSRs. Twelve landing ellipses located between latitudes 67–74°S have been proposed previously, using LEND data to estimate the H abundance from orbit (Mitrofanov et al., 2016). Ellipse 11 on the floor of Boguslawski Crater was initially selected as the most appropriate landing site candidate (e.g., Ivanov et al., 2015) but was later discarded as it did not appear to present the best characteristics in terms of Earth and Sun visibility.

We carried out a new study of possible landing ellipses using the previously listed constraints translated into our GIS. To build on previous work by Mitrofanov et al. (2016), we used both LPNS and LEND H abundance estimates and favored ellipses, which showed enhanced values in both datasets. By eliminating all areas with a slope $> 7^\circ$ and illumination $< 40\%$ (blackened on Fig. 3b), the same twelve ellipses initially identified, together with six additional candidate ellipses (labeled from 13 to 18), can be outlined in the remaining, H-rich terrains (Fig. 3a,b,c; Flahaut et al., 2016c).

Zonal statistics were then performed to compute mean values and standard deviations for the elevation, slope, illumination, Earth visibility, H abundance, minimum, maximum and average temperature, composition and age of each of the 18 proposed ellipses (Table 1, Table S1). There are discrepancies between the H abundance estimates from the LPNS and LEND but some ellipses (e.g., 1, 16) have high H abundance values

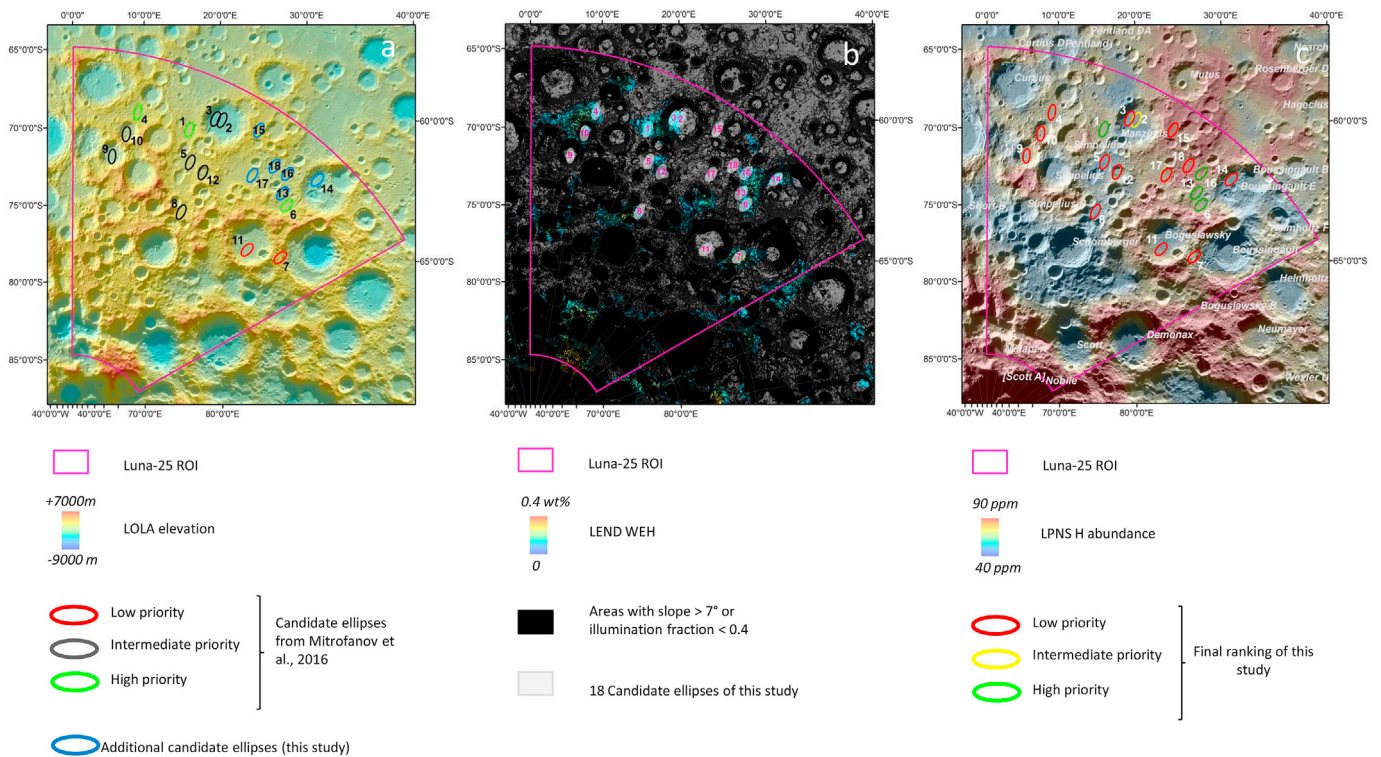


Fig. 3. Location of the 18 candidate ellipses within the region of interest for Luna-25 (magenta outline). A) Previous proposed ellipses described in [Mitrofanov et al. \(2016\)](#), and additional ones from this study are displayed on the LOLA topographic map. b) Comparison of the ellipses locations and the LEND H-rich regions. c) Comparison of the ellipses locations and the LPNS H-rich regions. All maps are overlain in transparency over the LROC WAC global mosaic and presented in polar stereographic projection.

according to data from both instruments. All the ellipses fall within the same average temperature range as estimated from the Diviner bolometric temperatures polar maps. Terrains within the landing ellipses appear rather homogeneous despite various ages (from Imbrian to pre-Nectarian), and appear to be composed of anorthositic material according to the Clementine false color RGB maps (e.g., [Heather and Dunkin, 2002](#)).

Ellipses 1, 6, 13 and 16 appear to have more desirable average values than other ellipses according to the computed statistics. Ellipse 1, which presents slightly better illumination conditions (47%), is considered a high priority site and has been studied at higher resolution by [Ivanov et al. \(2017\)](#) together with ellipses 4 and 6. All of the ellipses 1, 6, 13, and 16 are likely to be dominated by SPA basin ejecta, with local contributions from large, ancient craters such as Manzinus and Schomberger in ellipse 1, and Boguslawsky and Boussingault in ellipses 6, 13 and 16 ([Ivanov et al., 2017, Fig. 3c](#)). However, as noted by [Ivanov et al. \(2017\)](#), materials ejected by Boguslawsky and Boussingault from the lower portions of the SPA ejecta blanket form a smooth, hilly unit in ellipses 6, 13 and 16 that appear safer for landing than the flat plains of ellipse 1, as it is less populated by steep-walled craters.

5.2. The Luna-27 mission

The Russian led Luna-Resurs, or Luna-27, solar-powered mission will be tasked to detect and characterize lunar polar volatiles, including water ice, near the South Pole (e.g., [Mitrofanov et al., 2012b](#)). Luna-27 is planned as the first step towards a future automated Russian polar sample return mission (<http://www.iki.rssi.ru/eng/moon.htm>) and consists in a lander initially aimed at landing at latitudes $>80^\circ$.

Official requirements for landing site selection have not been released yet, but from the mission's objective and design, and the previous Luna missions, we infer the following constraints for the purposes of this analysis:

- Surface slopes at the landing site must not exceed 7° on a 2.5 m scale (or at the best available scale);
- The mean illumination within the landing area must be maximal;
- The Earth visibility (for radio communication) within the landing area must be maximal;
- The hydrogen abundance as estimated from orbit must be maximal;
- The surface temperature must be sufficiently low to allow for the presence of water ice at or near the surface.

Considering the previous constraints, all areas with average surface temperature >110 K or surface slope $>7^\circ$ at 20 m (the best LOLA DEM available for latitudes $\geq 80^\circ$) were discarded. By arbitrarily requiring the thresholds for the illumination fraction to be $>25\%$ and those for H abundances to be >100 ppm, only 14 candidate landing sites are retained ([Table 2, Fig. 4a](#)). Zonal statistics were then performed to compute mean values and standard deviations for the extent, slope, illumination, Earth visibility, H abundance, average temperature and surface age ([Table 2, Table S2](#)). Five of the proposed sites (labeled 9, 11, 12, 13, 14) are centered on the farside and offer less than 30% Earth visibility, implying that the mission would have to be assisted for operations via a relay orbiter ([Fig. 4b, Table 2](#)). Assuming a landing ellipse size that is at least $30 \text{ km} \times 15 \text{ km}$ in size (based on the Luna-Glob ellipse size), only three broad landing areas can be targeted near the South Pole: the plains of Ibn Bajja (site 6 of [Fig. 4](#)), the southern part of Amundsen crater (site 1, [Fig. 4](#)), and the farside location south of Wiechert J. crater (site 14, [Fig. 4](#)). Those three areas present low slopes over areas between 920 and 2150 km^2 . Diviner average surface temperature varies between 37 and 140 K spatially, suggesting that polar ice might not be ubiquitously present at the surface within these areas, but could be present at the subsurface. However, numerous colder areas and small scale PSRs are present. Among the three areas of larger extent, the plains south and west of the 12 km diameter Ibn Bajja crater offer the best compromise between all criteria with an average illumination fraction of 27%, average Earth

Table 1

Mean values of selected parameters, obtained for each of the Luna-25 18 proposed ellipses. Green and red colors highlight excellent and poor values respectively. Only ellipses 1, 2, 6, 13, and 16 fit all of the criterias listed above, the other ellipses fail at least one of those. However ellipse 2 has the worst illumination conditions and lowest H abundance, as estimated from orbit, compared to the other ones and is therefore listed as of intermediate priority. Standard deviation (STD) values are presented in [Table S1](#).

Ellipse #	Center longitude	Center latitude	Earth Visibility	Illumination fraction	H abundance from LPNS (ppm)	WEH from LEND (%)	LOLA elevation (m)	LOLA slope at 60 m (°)	Avg T from Diviner (°K)	Geol. unit	Unit description	Proposed priority ranking
1	21.21	-68.78	1.00	0.47	62	0.13	688	7.6	165	Ntp	Nectarian terra mantling and plains material	high
2	25.69	-67.38	1.00	0.43	43	0.08	-2499	6.2	162	Ip	Imbrian plains material	intermediate
3	24.61	-67.49	1.00	0.42	45	0.13	-2536	5.8	161	Ip	Imbrian plains material	low
4	11.57	-68.66	0.98	0.46	57	0.11	828	8.3	162	Ip	Imbrian plains material	low
5	23.66	-70.70	1.00	0.46	41	0.00	938	7.8	160	Ntp	Nectarian terra mantling and plains material	low
6	43.58	-69.55	1.00	0.45	78	0.12	460	9.5	161	pNbr	pre-Nectarian basin material, rugged	high
7	50.13	-72.16	0.92	0.44	69	0.19	2068	16.9	165	pNc	pre-Nectarian crater material	low
8	26.39	-73.88	0.99	0.43	37	0.08	1772	10.3	154	Isc	Imbrian secondary crater material	low
9	8.21	-71.73	1.00	0.41	64	0.00	-819	9.1	155	Esc	Erastosthenian secondary crater material	low
10	10.28	-70.15	1.00	0.41	74	0.14	119	15.5	165	Ec	Erastosthenian crater material, younger than most mare materials	low
11	43.94	-73.41	1.00	0.44	54	0.00	-872	6.4	158	Ntp	Nectarian terra mantling and plains material	low
12	26.74	-70.94	0.92	0.40	57	0.06	974	16.8	156	pNc	pre-Nectarian crater material	low
13	41.48	-69.17	0.99	0.46	66	0.06	353	9.0	163	pNb	pre-Nectarian basin materials	high
14	44.29	-67.02	0.99	0.43	42	0.11	-1959	8.0	165	pNc	pre-Nectarian crater material	low
15	31.79	-66.82	1.00	0.46	93	0.00	1542	7.9	166	pNt	pre-Nectarian terra material	intermediate
16	39.89	-68.01	0.99	0.47	84	0.10	377	9.0	159	pNb	pre-Nectarian basin materials	high
17	35.10	-69.45	0.99	0.47	74	0.00	623	9.2	160	pNb	pre-Nectarian basin materials	intermediate
18	37.33	-68.15	1.00	0.47	87	0.00	103	8.6	160	pNb	pre-Nectarian basin materials	intermediate

visibility of 37% and hydrogen abundance of ~110 ppm with LPNS and 0.12 wt% WEH with LEND. The highest H abundance from both LPNS and LEND data is expected at site 2 (Shoemaker-Faustini ridge), but illumination (25% on average) and slope (6.75° on average) are less optimal and the illuminated area is more restricted in extent (<200 km²) ([Table 2](#)). All 14 proposed sites present a variety of additional geologic features of interest, such as the possibility to analyze SPA ejecta in ancient pre-Nectarian units or to sample relatively young Upper Imbrian and Erastosthenian materials in the vicinity of Idel'son L (site 12), Wiechert J (site 14) or Shackleton (site 3).

5.3. The ESA Lunar Prospecting Rover (LPR) study into a mission

The LPR was an ESA study into a mission, consisting of a medium-class (<250 kg) rover mission to the South Pole of the Moon (e.g., [Carpenter et al., 2015](#); [Houdou et al., 2016](#)). The LPR main objective was to assess the distribution of water and other volatiles on a local scale during a 2-year mission (2022–2024). The rover model payload included a panoramic multispectral camera, a ground penetrating radar, a set of gamma-ray, neutron and IR spectrometers as well as a drill and a miniaturized chemical laboratory (PROSPECT). Mission requirements included a mobile range of 50 km, an average illumination fraction >0.25, and Earth visibility for direct-to-Earth communication (e.g., [Carpenter et al., 2015](#)).

Illumination conditions are found to be the main driver for the site selection here, as most areas around the South Pole do not meet the average sun visibility >25% criteria. Earth visibility, access to at least two small-scale PSRs, H abundance and access to several geologic units

along the possible traverse distance were used as additional criteria. Two potential sites were identified and correspond to sites that were also suggested for the Luna-27 mission: Site A (also listed as site 2 in [Table 2](#) for the Luna-27 mission, [Fig. 5](#)), the preferred site, is a H-rich (>150 ppm), topographic high between Shoemaker and Faustini craters; Site B (listed as site 6 in [Table 2](#) for the Luna-27 mission, [Figs. 4 and 6](#)) is situated in the Imbrian plain southwest of Ibn Bajja. In addition to fulfilling both scientific constraints and mission requirements, site A is:

- located at a geologic ‘triple point’ (where three different geological units meet),
- straddling a boundary between a high and low LEND H detection,
- located within an area where various ice stability depths are predicted and Diviner temperature is spatially variable.

The back-up site (site B) is in the plains around Ibn Bajja that appear to present good trafficability and average illumination, variable ice stability depths, variable (including low) surface temperatures, and access to two different geological units; however, average H abundances estimated from LPNS (From 95 to 127 ppm, 107 ppm on average) and LEND (From 0 to 0.23 wt%, 0.12 wt% on average) are relatively lower ([Flahaut et al., 2016 a,b](#); [Fig. 6](#)).

Detailed potential traverses were developed at site A based on high-resolution observations and other available datasets ([Figs. 5, 7 and 8](#)). Waypoints (WP) were defined in order to prepare for more complex traverses that will take hourly Earth visibility and illumination variations into account. The WP represent a nominal list of science stations where the rover would stop for sampling and measurements that cannot be done

Table 2

Mean values of selected parameters obtained for each of the Luna-27 14 proposed landing sites at latitudes >80°S (see selection criteria in section 5.2). Green and red colors highlight excellent and poor values respectively. All sites have pros and cons and offer access to various geologic materials. Site 2 and 6, which have good average values for each parameter presented here, were selected for the LPR case study presented in section 5.3. Standard deviation (STD) values are presented in Table S2.

site ID	Name	center lat.	center long.	area (km2)	avg Earth visibility	avg illum.	LPNS H (ppm)	LEND H (wt%)	slope at 20 m (°)	diviner avg T (K)	geol. unit	unit description
1	South Amundsen	-85.0	90.0	920	0.32	0.26	94	0.13	4.0	92	Ip (+Nc)	Plan material, Imbrian system (+ Nectarian floor and peak of the crater)
2	Shoemaker-Faustini ridge	-87.1	65.4	191	0.38	0.26	167	0.27	6.8	92	pNbr + pNc + Nc	Basin Material, Rugged, pre-Nectarian System + Crater Material Older Than Nectaris Basin, pre-Nectarian System + Crater Material Younger Than Nectaris Basin but Older Than Imbrium Basin, Nectarian System
3	Near Shackleton	-89.5	25.5	37	0.50	0.27	143	0.25	7.1	93	pNbr	Basin Material, Rugged, pre-Nectarian System
4	Faustini ridge	-87.6	103.7	101	0.31	0.26	149	0.29	6.1	84	pNbr	Basin Material, Rugged, pre-Nectarian System
5	Near Shackleton	-88.6	101.4	83	0.39	0.24	151	0.19	7.6	91	pNbr (+Ec)	Basin Material, Rugged, pre-Nectarian System + Erastosthenian material of Shackleton
6	South / West Ibn Bajja	-86.4	-86.7	2146	0.37	0.27	107	0.12	4.8	92	Ip + pNbr	Plan material, Imbrian system + Basin Material, Rugged, pre-Nectarian System
7	South Cabeus B.	-84.0	-60.5	75	0.55	0.28	158	0.05	4.6	98	pNbr	Basin Material, Rugged, pre-Nectarian System
8	North de Gerlache	-87.9	-65.1	30	0.50	0.32	137	0.28	6.0	95	pNbr	Basin Material, Rugged, pre-Nectarian System
9	North Sverdrup	-87.4	-148.2	211	0.21	0.26	108	0.17	5.5	86	pNbr	Basin Material, Rugged, pre-Nectarian System
10	West Sverdrup	-88.0	173.2	75	0.33	0.29	136	0.23	5.9	84	pNbr	Basin Material, Rugged, pre-Nectarian System
11	South Wiechert P.	-87.2	146.7	243	0.26	0.28	131	0.23	4.5	83	Ntp	Terra-Mantling and Plains Material, Nectarian System
12	South Idel'son L.	-84.6	115.7	290	0.23	0.32	105	0.11	4.3	91	Ntp (+lc2)	Terra-Mantling and Plains Material, Nectarian System (+ Upper Imbrian material of Idel'son L crater)
13	West Amundsen	-85.8	112.7	188	0.23	0.37	99	0.11	4.1	99	Ntp	Terra-Mantling and Plains Material, Nectarian System
14	South Wiechert J.	-86.5	176.6	1691	0.08	0.29	99	0.19	5.0	91	Ntp (+Ec)	Terra-Mantling and Plains Material, Nectarian System + Erastosthenian material of Wiechert J crater

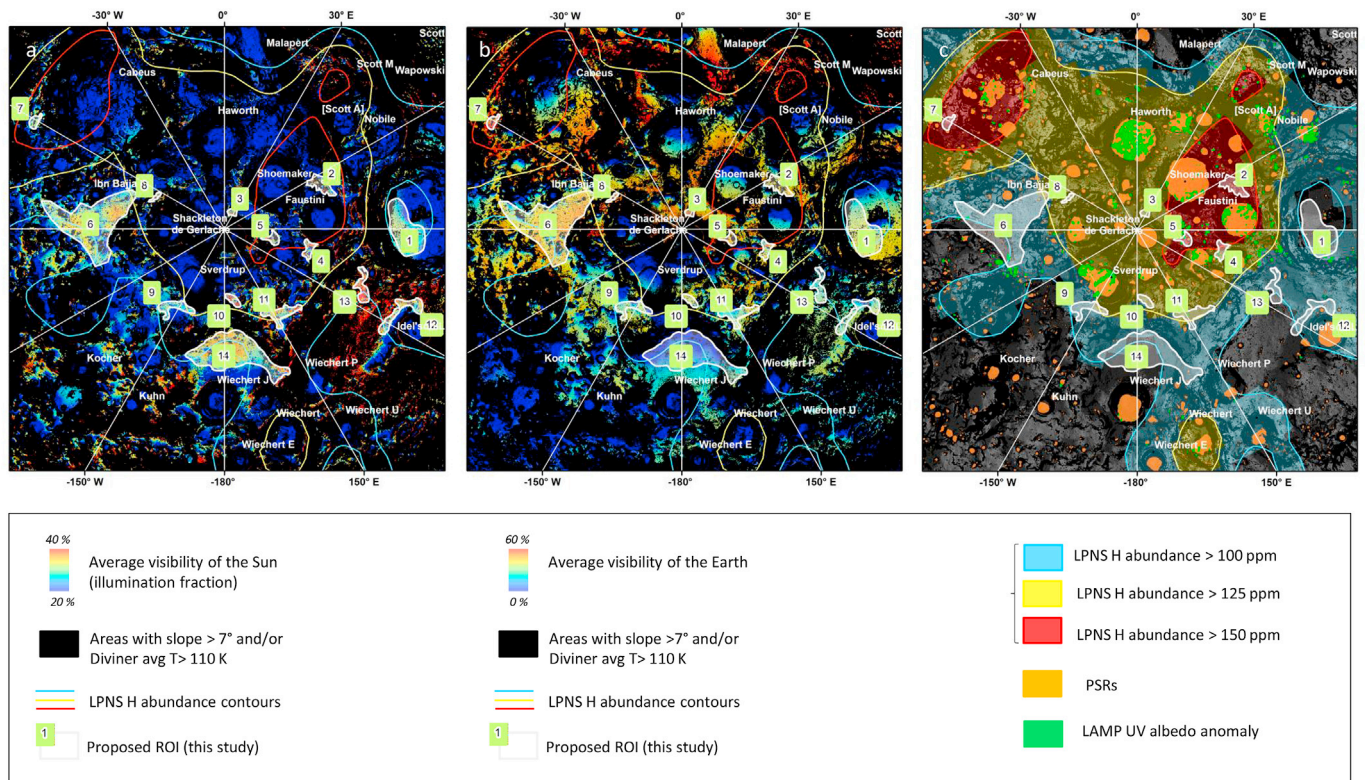


Fig. 4. Location of the 14 candidate landing sites for a Luna-27 type mission aimed at investigating polar volatiles at southern high latitudes (>80°). A) Proposed ROIs of relatively high illumination (>25%) and elevated H (>100 ppm) are indicated (white outlines), areas of Diviner average temperature > 110K and/or slope values > 7° were blackened. The background is the average visibility of the Sun map from Mazarico et al. (2011). b) Same as a), but with the background is the average visibility of the Earth map from Mazarico et al. (2011). c) The proposed sites are displayed over the LPNS H abundance data and compared to LAMP UV anomalies and PSRs locations (please refer to the text for data sources).

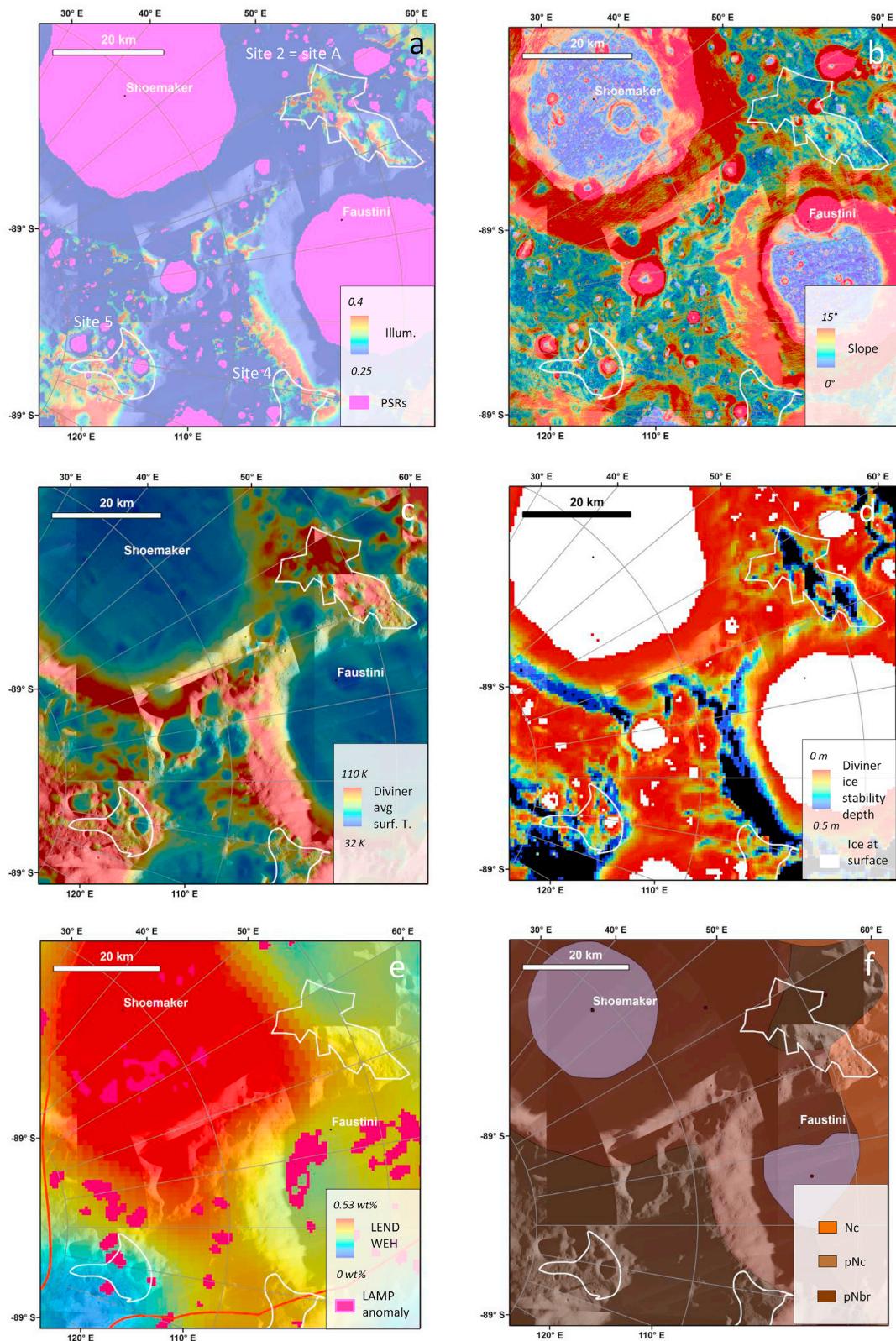


Fig. 5. Close-up of LPR site A, the Shoemaker-Faustini ridge. The white outlines represent the areas of higher illumination, low slope and low diviner T as described in section 5.2 (Sites 2, 4, and 5 are shown on this close-up). The data is shown in transparency over LRO WAC + NAC polar mosaics P870S0450, P870S0750, P870S1050, P880S0225, P880S0675, P880S1125, P892S0450 and P892S1350. A) Illumination map, b) Slope map, c) Diviner average annual surface temperature map, d) Ice stability depth map, as predicted by Diviner thermal models, e) LEND hydrogen abundance map. The 150 ppm H abundance limit of LPNS is indicated as a red line as in previous figures. LAMP UV albedo anomalies (which may indicate the presence of surface frost) are also represented. F) Geological map (for data sources, please refer to section 2: Datasets and method). (For interpretation of the references to color in this figure legend, the reader is referred to the Web version of this article.)

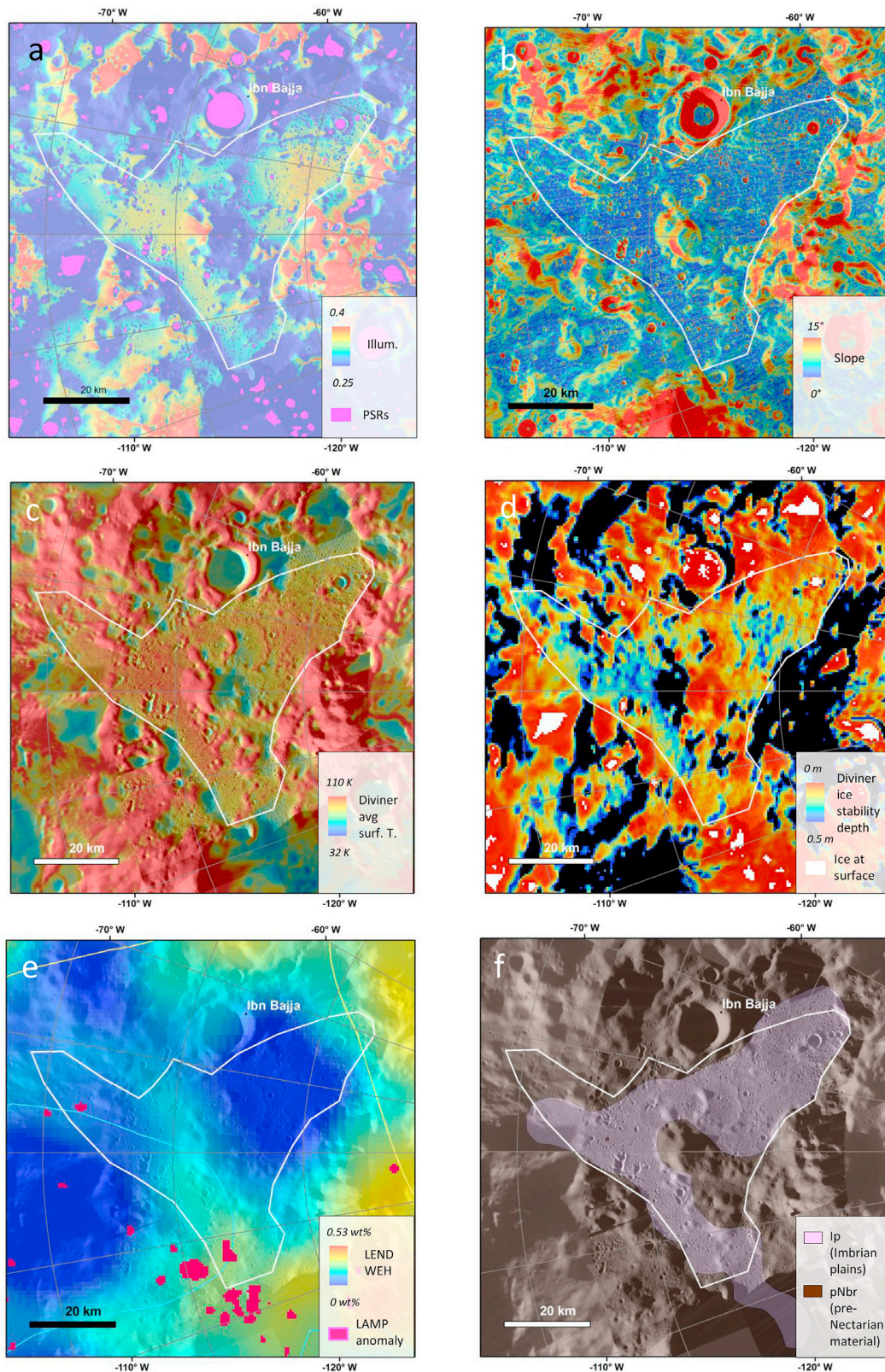


Fig. 6. Close-up of LPR site B, the Ibn Bajja plains. The white outline represents the areas of higher illumination, low slope and low diviner T drawn in section 5.2. The data is shown in transparency over LRO WAC + NAC polar mosaics P860S2587, P860S2812, P870S2550 and P870S2850. A) Illumination map, b) Slope map, c) Diviner average annual surface temperature map, d) Ice stability depth map, as predicted by Diviner thermal models, e) LEND hydrogen abundance map. The 100 and 125 ppm H abundance limits of LPNS are indicated as blue and yellow lines respectively. LAMP UV albedo anomalies (which may indicate the presence of surface frost) are also represented and present within the area. F) Geological map (for data sources, please refer to section 2: Datasets and method). (For interpretation of the references to color in this figure legend, the reader is referred to the Web version of this article.)

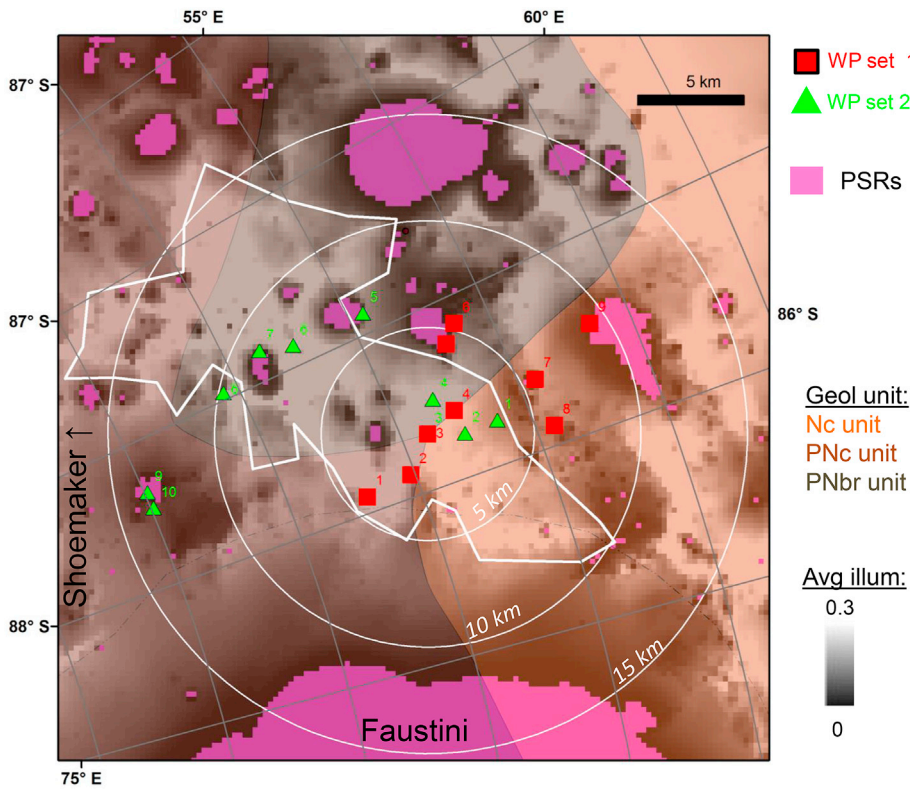


Fig. 7. Examples of waypoints that could be used to establish a traverse at LPR test site A. Waypoints were defined as possible ground stations where different conditions are expected and where various parameters could be measured. Two sets of waypoints (green triangles and red squares) starting from WP3 – the intersection of three geologic units – are shown here. The white outline indicates LPR site A (Fig. 5). White circles represent a 5, 10 and 15 km buffer zone away from WP3. Both traverses extend beyond the area of higher illumination towards PSRs and represent a minimum path of 22 km (WP set 1) and 25 km (WP set 2) respectively. (For interpretation of the references to color in this figure legend, the reader is referred to the Web version of this article.)

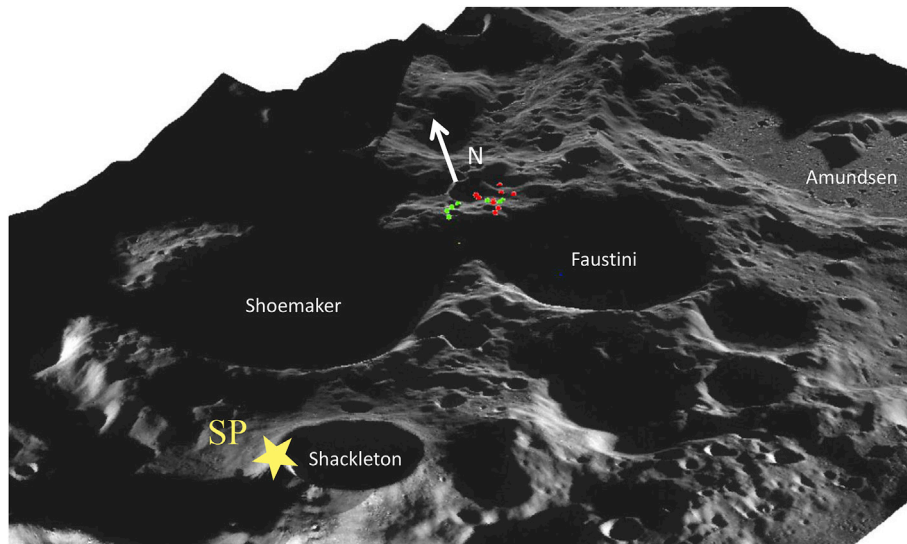


Fig. 8. 3D view of the South Pole area with WP sets 1 (red) and 2 (green). LROC WAC data at 100m/pixel are projected using LOLA 80 S DEM at 20m/pixel as base height. (For interpretation of the references to color in this figure legend, the reader is referred to the Web version of this article.)

while driving, and that would be necessary to fully achieve the mission's science goals. The WP selection was defined in order to encompass:

- The contact between the three geological units (1 WP),
- At least 2 WP per geological unit,
- At least 3 WP in different PSRs,
- At least 2 WP in areas where the maximum T does not exceed 110K,
- At least 2 WP each in areas where ice stability depth is predicted to be equal to 0, between 0.01 and 0.25 m, and 0.25–0.5 m,
- At least 1 WP in areas where ice stability depth is predicted to be between 0.5 and 1 m, > 1 m.

Two sets of way points are proposed, which would correspond, if following the shorter path (direct line), to traverses of 22 (9 WP, set 1) and 25 km (10 WP, set 2) (Fig. 7). It is not expected, in the proposed scenario, that the rover returns to its landing site at the end of the mission. WP sets are built around WP3, the geologic triple point, which is common to both traverses. The area of higher illumination defined as site A is spatially limited by the deep Faustini crater PSR to the east, Shoemaker crater deep PSR to the south, steep terrains to the north and less illuminated terrains to the west (Figs. 7 and 8). Proposed traverse egress up to 15 km away from WP3 into the north and west areas in WP set 1, to the west and south in set 2, to visit multiple, small-scale PSRs as well as

areas where water ice should crop out at the surface (Figs. 5 and 7, Table S3). Realistic traverses should account for the varying conditions and preferred slope rather than the shortest path between WPs. Accessibility maps for the years 2022–2024 were derived in accompanying studies (e.g., Diederich et al., 2016; Ferri et al., 2016) to select the most appropriate route as the Earth and Sun position vary. These supplementary studies showed that it is possible to connect the stations while maximizing both the illumination of the site (to supply sufficient energy to the solar-powered rover) as well as good communication windows with Earth (to provide robust teleoperation), but with the planned design the rover would have to keep chasing the light in order to operate and survive.

6. Discussion

6.1. Candidate landing sites for volatile investigations at high latitudes

A wide range of remote sensing datasets is now available and can be explored simultaneously in multi-parameter analyses to optimize the selection of landing sites for future lunar missions. Following this approach, we identified eleven areally broad ROIs that appear suitable for landing and general science investigations of polar volatiles, followed by more specific landing sites that meet the mission requirements for Luna-25, Luna-27 and LPR missions. All of the proposed landing sites for the polar missions (Luna 27 and LPR study) encompass the 11 ROI that were previously defined in this study, but extent beyond the ROI previously defined by LEAG VSAT team, 2015 and Lemelin et al. (2014). Most of the proposed landing sites are located within the ROIs of higher latitudes, in the vicinity of the South Pole. These example studies indicate that several factors can limit the possible areas of exploration, such as the Sun and Earth visibilities. Luna-25 candidate sites are all limited to latitudes $<70^\circ$ on the nearside in order to meet high values for both criteria, therefore limiting this mission to the investigation of non-polar volatiles (see section 5.1). The same region was considered for the landing site of the Indian space research organization Chandrayaan-2 lander and rover due to the same restrictions on power and communication (e.g., Amitabh et al., 2018). Our study shows that, in the best-case scenarios, areas of acceptable slope and surface temperatures at latitudes $>80^\circ$ would not offer more than $\sim 35\%$ illumination and/or 50% Earth visibility. Such values pose challenges for long-term operations of solar-powered missions. Most of the suitable sites with illumination $>25\%$ (see section 5.2) are of relatively minor spatial extent (30 to a few 100 km^2) and will require precise landing and small landing ellipse requirements. If we consider an ellipse size similar to that of Luna-25, only three possible landing areas were identified at latitudes exceeding 80° : the plains of Ibn Bajja, the southern part of Amundsen crater and the farside location south of Wiechert J crater. These landing site encompasses two new ROIs defined in this study. However, surface temperature and H abundances in these areas vary spatially, and water ice will likely not be present within the entire area. These broad areas may therefore be better suited for a rover mission, such as the LPR mission, which can reach nearby cold traps, rather than a static lander.

It is important to note that further reduced areas ($<1 \text{ km}^2$) of higher illumination ($>78\%$) have been identified on the rims of impact craters near the South Pole (Mazarico et al., 2011, Figs. S1 and S2). However, the most illuminated areas are presumably too hot to contain near-surface volatiles and therefore less interesting for scientific investigations (Fig. S2). These areas could however represent interesting power stations for more complex mission scenarios, assuming that high-precision landing ($<a \text{ few } 100 \text{ m}$) can be achieved. Our results further demonstrate that it is virtually impossible to find an area of illumination $>25\%$ where water ice should be stable at the surface according to the available LOLA-based illumination and Diviner thermal models (Fig. 1c, g). However, in these locations, water ice and other volatiles are expected to be stable at shallow depths (from a few 10 's of cm to meters, Paige et al., 2010) and could be accessed with a scoop or drill system.

6.2. The potential for additional science benefits

Lunar polar areas remain unexplored and represent key sites to address some of the top science priorities of future lunar exploration (e.g., Crawford et al., 2012; NRC, 2007). In addition to investigating polar volatiles (science concept 4 of the NRC, 2007 report), some of the top science priorities identified by the community (NRC, 2007) can be investigated at the South Pole specifically – as it lies within the SPA basin (e.g., Science concept 1,2,3,5, see Kring and Durdas, 2012; Flahaut et al., 2012). SPA is indeed the largest and oldest known impact structure on the Moon, and its extent suggests that it may have excavated the lunar lower crust and mantle, providing a window into the lunar interior, and access to primary products of the lunar magma ocean crystallization (NRC science concepts 2 and 3). Dating SPA formation (NRC concept 1) is the top-priority of the NRC (2007) report as it could help anchor the period of basin formation on the Moon, and would allow to test the lunar cataclysm hypothesis, but the collected samples would have to be returned back to Earth for analysis, which is not planned for Luna-25, Luna-27 and the LPR missions.

The area that we surveyed around the South Pole is referred to as part of SPA's "heterogeneous annulus", which is defined as spatially interspersed feldspathic and (minor) mafic materials comprised within the basin outer part (e.g., Moriarty and Pieters, 2018). The non-mare mafic components of this heterogeneous annulus are dominated by Mg-pyroxene signature, which might be indicative of SPA melt and/or lower crust/mantle components (Moriarty and Pieters, 2018). Mapping the occurrence of mafic minerals in the polar regions with remote sensing VNIR spectrometers is however challenging because of the low illumination, and hence the low signal-to-noise ratio of the instruments. Accessing these key samples might also be difficult as they may have been brecciated and covered by subsequent impact ejecta. Whereas the Malapert massifs likely represent SPA rim (and therefore, highland crust covered in SPA ejecta), Shackleton crater and the South Pole might be located on an inner ring on SPA, which uplifted deeper material (Spudis et al., 2008). Together with the Amundsen crater central peak, which is expected to contain material from depths $<16 \text{ km}$, the Shackleton crater, De Gerlache crater, and their surroundings represent promising sites for SPA investigations near the South Pole.

The detailed geological record preserved in the near sub-surface at various candidate landing sites is expected to vary. In addition to ancient SPA - derived material, dating Erastosthenian samples from young polar craters such as Wiechert J., or well-defined units like unit Nc at site 2 (Nc is a Nectarian unit that is well-bracketed in terms of stratigraphy: it is stratigraphically younger than Nectaris basin but older than Imbrium basin) would be of great additional science benefit as it would enable the establishment of a more precise lunar chronology. Measuring volatile elements in relatively young, or only recently exposed materials could also help determine the relative contribution of indigenous and exogenous volatiles (Füri et al., 2017, 2019). More work is required to define the geologic contexts, and likely sub-surface environments, of all potential south polar landing sites as part of a detailed site selection process. Still, additional geologic investigations of various types appear to be possible at many sites.

6.3. Implications for future missions

Existing datasets suggest that there are no flat areas $>1 \text{ km}^2$ with illumination $\geq 50\%$ at latitudes $>80^\circ$. This will impact the design and/or duration of future polar missions. Only three elevated locations around Nobile crater show $\sim 50\%$ average illumination over a 1 km radius circle, but these areas are steep and likely too warm for water ice to be present at or near the surface (Figs. S1 and S2). Due to the rough topography of the South Pole, Earth visibility is also limited and does not reach 100% at latitudes $>86^\circ$, even on the nearside, which implies that future missions to the pole will either require more autonomy or mandatory "naps".

Areas of more limited illumination ($<35\%$) were identified in our

study (Table 2), but targeting these areas will require precise landing (as they are limited in extent, and generally $<200 \text{ km}^2$) and/or access to the shallow subsurface for volatile sampling using drills (as their surface temperature might be too elevated for water ice to outcrop).

Without nuclear power, it is virtually impossible for a lander mission to directly investigate cold-trap PSRs where water ice is expected to be stable at the surface, but it might be possible to land in a partially illuminated/partially shadowed crater such as Amundsen, and investigate the colder areas with a rover, as suggested by Lemelin et al. (2014). However, rover missions at the pole will be challenged by the rough topography at most locations, and the necessity to constantly track the light, if solar-powered. Rechargeable hoppers are being considered for the Chinese polar exploration program and might represent a tempting alternative to a purely static or mobile mission (e.g., Xu et al., 2019).

Current understanding of the spatial variation of volatile abundances at the scale of landers is a major uncertainty and is a strong limitation for the use of static landers, as they could land on a volatile-free area within a broader H-rich region. Nonetheless, missions to the lunar poles are key for ground-truthing the recent detections and predictions of hydrogen enrichments, and to answer a number of fundamental strategic knowledge gaps, such as the nature and distribution of polar volatiles, but also the physical and thermal properties of the polar soil and regolith (NRC, 2007; ESA, 2019). Robotic precursor missions such as those described in this study will be key to pave the way towards a potential lunar base, or renewed manned exploration, which are both envisioned at the South Pole in the next decade.

7. Conclusions

We identified eleven general regions of interest near the South Pole that would allow conducting volatiles and geologic investigations. These regions have enhanced hydrogen abundances ($H > 100 \text{ ppm}$) and temperature regimes that allow water ice to be stable at or near the surface (Diviner average annual temperature $<110 \text{ K}$). Compelling evidence for water ice at or near the surface has been reported in these ROIs by various orbital instruments (e.g., Hayne et al., 2015; Fisher et al., 2017; Li et al., 2018). These ROIs include a broad area ($>200 \text{ km} \times 200 \text{ km}$) around the lunar South Pole, together with smaller regions near Cabeus, Amundsen, Ibn Bajja, Wiechert J and Idel'son craters. Three of these ROIs were also previously identified by Lemelin et al. (2014) and LEAG VSAT team (2015) (the area near the South Pole, Amundsen and Cabeus craters) and eight are new, based on our revised set of constraints and the availability of recent data analyses conducted using LAMP, LOLA and M^3 data. These ROIs may be key targets for future polar missions. The rich science potential of these ROIs is increased by the possibility to sample South Pole Aitken basin heterogeneous annulus (which may contain excavated lunar mantle material), and to date several key events spanning most of the Moon's history through sample return missions.

Selecting more specific landing sites is highly mission dependent, and strongly limited by Earth and Sun visibility in the case of solar powered-missions and/or missions without relay orbiters. Indeed, we performed a detailed landing site analysis for missions with characteristics approximating those of Luna-25, Luna-27 and LPR missions and obtained different results. We found that most potentially volatile-bearing outcrops are not accessible to these missions because of the low average illumination at the volatile-rich locations (e.g., PSRs); however, if not cropping out at the surface, water ice should be present within the first meter of the surface at the sites proposed for Luna-27 and LPR like missions. These sites include the ridge between Faustini and Shoemaker craters (labeled as site A or site 2 in our studies), where expected H abundances are $> 150 \text{ ppm}$, average illumination $\sim 26\%$, average Earth visibility $\sim 38\%$, average surface temperature $\sim 92 \text{ K}$ (but highly variable) and average slope $< 7^\circ$. We propose possible waypoints for a rover traverse at this site, and show that access to small-scale PSRs within areas of enhanced illumination is possible with mobility.

Site A is however of limited extent, implying that precise landing will

be required to investigate this area. The plains of Ibn Bajja, presented as site B or site 6, are more extensive in area, but they are characterized by highly variable and, on average, lower surface temperatures and H abundances, suggesting that this area is not well-suited for static lander missions. The present study shows that there is no single or simple scenario for *in situ* analyses and sampling of lunar polar volatiles with solar-powered missions, and that trade-off in mission design and scenarios will have to be considered. The use of relay orbiters may benefit future missions by extending the possibility of landing sites to farside locations.

Acknowledgments

The authors wish to thank Erwan Mazarico for kindly sharing his data, as well as the editor and anonymous reviewers for helpful comments. The authors are also grateful to ESA and the ESA topical team on the exploitation of local planetary material for insightful discussions. This study is supported by the CNES "Appel à Projets de Recherche" Luna attributed to J. Flahaut. M. Anand acknowledges support from UKSA and STFC grants (#ST/P000657/1 and # ST/R001391/1, resp.). W. van Westrenen acknowledges financial support from a Netherlands Organisation for Scientific Research Vici award and from the Netherlands Space Office. This is CRPG contribution N°2718.

Appendix A. Supplementary data

Supplementary data to this article can be found online at <https://doi.org/10.1016/j.pss.2019.104750>.

References

- Amitabh, S., Srinivasan, T.P., Suresh, K., 2018. Potential landing sites for Chandrayaan-2 lander in southern hemisphere of moon. In: Lunar and Planetary Science Conference, vol 49, p. 2083.
- Anand, M., Tartèse, R., Barnes, J.J., 2014. Understanding the origin and evolution of water in the Moon through lunar sample studies. *Phil. Trans. R. Soc. A* 372 (2024), 20130254.
- Anand, M., Crawford, I.A., Balat-Pichelin, M., Abanades, S., van Westrenen, W., Péraudeau, G., Jaumann, R., Seboldt, W., 2012. A brief review of chemical and mineralogical resources on the Moon and likely initial *in situ* resource utilization (ISRU) applications. *Planet. Space Sci.* 74 (1), 42–48.
- Anand, M., 2010. Lunar water: a brief review. *Earth Moon Planets* 107, 65–73.
- Arnold, J.R., 1979. Ice in the lunar polar regions. *J. Geophys. Res.* 84, 5659–5668.
- Bussey, D.B.J., McGovern, J.A., Spudis, P.D., Neish, C.D., Noda, H., Ishihara, Y., Sørensen, S.-A., 2010. Illumination conditions of the South Pole of the Moon derived using Kaguya topography. *Icarus*. <https://doi.org/10.1016/j.icarus.2010.03.028>.
- Bussey, D.B.J., Lucey, P.G., Steutel, D., Robinson, M.S., Spudis, P.D., Edwards, K.D., 2003. Permanent shadow in simple craters near the lunar poles. *Geophys. Res. Lett.* 30, 1278. <https://doi.org/10.1029/2002GL016180>.
- Bussey, D.B.J., Spudis, P.D., Robinson, M.S., 1999. Illumination conditions at the lunar South Pole. *Geophys. Res. Lett.* 9, 1187–1190.
- Carpenter, J.D., Fisackerly, R., Aziz, S., Houdou, B., 2015. Exploring cold trapped volatiles from stationary landers and mobile rovers: ESA activities for resource prospecting at the Poles. In: Annual Meeting of the Lunar Exploration Analysis Group, vol 1863, p. 2027.
- Cintala, M.J., Grieve, R.A., 1998. Scaling impact melting and crater dimensions: implications for the lunar cratering record. *Meteorit. Planet. Sci.* 33 (4), 889–912.
- Colaprete, A., et al., 2010. Detection of water within the LCROSS ejecta plume. *Science* 330, 463–468. <https://doi.org/10.1126/science.1186986>.
- Crawford, I.A., Anand, M., Cockell, C.S., Falcke, H., Green, D.A., Jaumann, R., Wiczeorek, M.A., 2012. Back to the Moon: the scientific rationale for resuming lunar surface exploration. *Planet. Space Sci.* 74 (1), 3–14.
- De Rosa, D., Bussey, B., Cahill, J.T., Lutz, T., Crawford, I.A., Hackwill, T., van Gasselt, S., Neukum, G., Witte, L., McGovern, A., Grindrod, P.M., Carpenter, J.D., 2012. Characterisation of potential landing sites for the European space agency's lunar lander project. *Planet. Space Sci.* 74, 224–246.
- Diedrich, T., et al., 2016. Prospecting and Returning Lunar Surface Samples with Volatiles. 4th European Lunar Symposium abstract #031.
- Elphic, R.C., Eke, V.R., Teodoro, L.F.A., Lawrence, D.J., Bussey, D.B.J., 2007. Models of the distribution and abundance of hydrogen at the lunar South Pole. *Geophys. Res. Lett.* 34 (13).
- ESA, 2019. ESA strategy for science at the moon. available at: ESA. <http://exploration.esa.int/jump.cfm?oid=61371>.
- ESA TT ELP, Topical Team on the Exploitation of Local Planetary Material, 2015. A 'European Response' to the Recent Lunar Exploration and Analysis Group (LEAG) Volatiles Special Action Team (VSAT) Report on Lunar Volatiles (available at: ISECG).
- Feldman, W.C., Maurice, S., Lawrence, D.J., Little, R.C., Lawson, S.L., Gasnault, O., Wiens, R.C., Barraclough, B.L., Elphic, R.C., Prettyman, T.H., Steinberg, J.T.,

- Binder, A.B., 2001. Evidence for water ice near the lunar poles. *J. Geophys. Res.* 106, 23231–23252.
- Ferri, A., et al., 2016. Lunar Volatile Prospector Mission. 4th European Lunar Symposium abstract #079.
- Fisher, E.A., Lucey, P.G., Lemelin, M., Greenhagen, B.T., Siegler, M.A., Mazarico, E., Aharonson, O., Williams, J.-P., Hayne, P.O., Neumann, G.A., Paige, D.A., Smith, D.E., Zuber, M.T., 2017. Evidence for surface water ice in the lunar polar regions using reflectance measurements from the Lunar Orbiter Laser Altimeter and temperature measurements from the Diviner Lunar Radiometer Experiment. *Icarus* 292, 74–85.
- Flahaut, J., et al., 2016a. Regions of Interest for Lunar Volatiles Investigations : a European Perspective. ISECG Lunar Polar Volatiles Virtual Workshop #2 (hosted by the NASA SSERVI).
- Flahaut, J., et al., 2016b. Candidate Landing Sites Near the Lunar Poles : a European Perspective. 4th European Lunar Symposium abstract #004.
- Flahaut, J., et al., 2016c. Candidate Landing Sites for the Luna-Glob Mission, 7ms3 symposium, abstract # 7MS3-MN-10.
- Flahaut, J., Blanchette-Guertin, J.F., Jilly, C., Sharma, P., Souchon, A., Van Westrenen, W., Kring, D.A., 2012. Identification and characterization of science-rich landing sites for lunar lander missions using integrated remote sensing observations. *Adv. Space Res.* 50 (12), 1647–1665.
- Fortezzo, C.M., Hare, T.M., 2013. Completed digital renovation of the 1: 5,000,000 lunar geologic map series. In: Lunar and Planetary Science Conference, vol 44, p. 2114.
- Füri, E., Zimmermann, L., Deloule, E., Saal, A.E., 2019. The H-noble gas signature of single apollo volcanic glass beads. In: Lunar and Planetary Science Conference, vol 50 abstract #1778.
- Füri, E., Deloule, E., Trappitsch, R., 2017. The production rate of cosmogenic deuterium at the Moon's surface. *Earth Planet. Sci. Lett.* 474, 76–82.
- Füri, E., Marty, B., 2015. Nitrogen isotope variations in the solar system. *Nat. Geosci.* 8, 515–522.
- Gladstone, G.R., et al., 2012. Far-ultraviolet reflectance properties of the Moon's permanently shadowed regions. *J. Geophys. Res.* 117. <https://doi.org/10.1029/2011JE003913>.
- Gladstone, G.R., Stern, S.A., Retherford, K.D., Black, R.K., Slater, D.C., Davis, M.W., Versteeg, M.H., Persson, K.B., Parker, J.W., Kaufmann, D.E., Egan, A.F., 2010. LAMP: the Lyman alpha mapping project on NASA's Lunar reconnaissance orbiter mission. *Space Sci. Rev.* 150 (1–4), 161–181.
- Gläser, P., Oberst, J., Neumann, G.A., Mazarico, E., Speyerer, E.J., Robinson, M.S., 2018. Illumination conditions at the lunar poles: implications for future exploration. *Planet. Space Sci.* 162, 170–178.
- Gläser, P., Scholten, F., De Rosa, D., Marco Figuera, R., Oberst, J., Mazarico, E., Neumann, G.A., Robinson, M.S., 2014. Illumination conditions at the lunar South Pole using high resolution Digital Terrain Models from LOLA. *Icarus* 243, 78–90.
- Hayne, P.O., et al., 2019. Carbon dioxide frost at the poles of the Moon: thermal stability and observational evidence from the lunar reconnaissance orbiter. In: Lunar and Planetary Science Conference, vol 50. LPI Contrib. No. 2132.
- Hayne, P.O., Hendrix, A., Sefon-Nash, E., Siegler, M.A., Lucey, P.G., Retherford, K.D., Williams, J.P., Greenhagen, B.T., Paige, D.A., 2015. Evidence for exposed water ice in the Moon's south polar regions from Lunar Reconnaissance Orbiter ultraviolet albedo and temperature measurements. *Icarus* 255, 58–69.
- Heather, D.J., Dunkin, S.K., 2002. A stratigraphic study of southern Oceanus Procellarum using Clementine multispectral data. *Planet. Space Sci.* 50 (14–15), 1299–1309.
- Houdou, B., et al., 2016. Building ESA's Lunar Exploration Mission Capabilities, 4th European Lunar Symposium, abstract #051.
- Ingersoll, A. P.T. Svitek, Murray, B.C., 1992. Stability of polar frosts in spherical bowl-shaped craters on the Moon, Mercury, and Mars. *Icarus* 100, 40–47.
- Ivanov, M.A., et al., 2017. Geological characterization of the three high-priority landing sites for the Luna-Glob mission. *Planet. Space Sci.* 162, 190–206.
- Ivanov, M.A., et al., 2015. Landing site selection for Luna-Glob mission in crater Boguslawsky. *Planet. Space Sci.* 117, 45–63.
- Kring, D.A., Durda, D.D., 2012. A Global Lunar Landing Site Study to Provide the Scientific Context for Exploration of the Moon. LPI Contribution, 1694.
- Lawrence, D.L., 2017. A tale of two poles: toward understanding the presence, distribution, and origin of volatiles at the polar regions of the Moon and Mercury. *J. Geophys. Res.* 122, 21–52.
- LEAG VSAT team, 2015. Volatiles specific action team final report. available at http://www.lpi.usra.edu/leag/reports/vsat_report_123114x.pdf.
- Lemelin, M., Lucey, P.G., Neumann, G.A., Mazarico, E.M., Barker, M.K., Kakazu, A., et al., 2016. Improved calibration of reflectance data from the LRO Lunar Orbiter Laser Altimeter (LOLA) and implications for space weathering. *Icarus* 273, 315–328.
- Lemelin, M., Blair, D.M., Roberts, C.E., Runyon, K.D., Nowka, D., Kring, D.A., 2014. High-priority lunar landing sites for in situ and sample return studies of polar volatiles. *Planet. Space Sci.* 101, 149–161.
- Li, S., Lucey, P.G., Milliken, R.E., Hayne, P.O., Fisher, E., Williams, J.-P., Hurley, D.M., Elphic, R.C., 2018. Direct evidence of surface exposed water ice in the lunar polar regions. *Proc. Natl. Acad. Sci.* 115 (36), 8907–8912.
- Lin, Y., van Westrenen, W., 2019. Isotopic evidence for volatile replenishment of the moon during late accretion. *Nat. Sci. Review* nwz033. <https://doi.org/10.1093/nsr/nwz033>.
- Lin, Y., Tronche, E.J., Steenstra, E.S., van Westrenen, W., 2017. Evidence for an early wet Moon from experimental crystallisation of the lunar magma ocean. *Nat. Geosci.* 10, 14–18.
- Lucey, P.G., et al., 2014. The global albedo of the Moon at 1064 nm from LOLA. *J. Geophys. Res. Planets* 119, 1665–1679. <https://doi.org/10.1002/2013JE004592>.
- Lucey, P.G., Blewett, D.T., Taylor, G.J., Hawke, B.R., 2000. Imaging of lunar surface maturity. *J. Geophys. Res.* 105.
- Margot, J.L., Campbell, D.B., Jurgens, R.F., Slade, M.A., 1999. Topography of the Lunar poles from radar interferometry: a survey of cold trap locations. *Science* 284, 1658–1660.
- Mazarico, E., Neumann, G.A., Smith, D.E., Zuber, M.T., Torrence, M.H., 2011. Illumination conditions of the lunar polar regions using LOLA topography. *Icarus* 211, 1066–1081.
- McGovern, J.A., Bussey, D.B., Greenhagen, B.T., Paige, D.A., Cahill, J.T.S., Spudis, P.D., 2013. Mapping and characterization of non-polar permanent shadows on the lunar surface. *Icarus* 223, 566–581.
- Mitrofanov, I., Djachkova, M., Litvak, M., Sanin, A., 2016. The Method of Landing Sites Selection for Russian Lunar Lander Missions, vol 18. abstr. p. EGU2016, 10018.
- Mitrofanov, I., Litvak, M., Sanin, A., Malakhov, A., Golovin, D., Boynton, W., Droege, G., Chin, G., Evans, L., Harshman, K., Fedosov, F., Garvin, J., Kozyrev, A., McClanahan, T., Milikh, G., Mokrousov, M., Starr, R., Sagdeev, R., Shevchenko, V., Shvetsov, V., Tretyakov, V., Trombka, J., Varenikov, A., Vostrukhin, A., 2012a. Testing polar spots of water-rich permafrost on the Moon: LEND observations onboard LRO. *J. Geophys. Res.* 117, 0.
- Mitrofanov, I.G., Zelenyi, L.M., Tretyakov, V.I., 2012b. Upgraded Program of Russian Lunar Landers: Studying of Lunar Poles. LEAG meeting abstract #3025.
- Moriarty, D.P., Pieters, C.M., 2018. The character of south Pole-Aitken basin: patterns of surface and subsurface composition. *J. Geophys. Res.: Planets* 123 (3), 729–747.
- Noda, H., et al., 2008. Illumination conditions at the lunar polar regions by KAGUYA (SELENE) laser altimeter. *Geophys. Res. Lett.* 35, 24203. <https://doi.org/10.1029/2008GL035692>.
- Nozette, S., Spudis, P.D., Robinson, M.S., Bussey, D.B.J., Lichtenberg, C., Bonner, R., 2001. Integration of lunar polar remote-sensing data sets: evidence for ice at the lunar South Pole. *J. Geophys. Res.: Planets* 106 (E10), 23253–23266.
- Nozette, S., Lichtenberg, C.L., Spudis, P., Bonner, R., Ort, W., Malaret, E., Robinson, M., Shoemaker, E.M., 1996. The Clementine bistatic radar experiment. *Science* 274, 1495–1498. <https://doi.org/10.1126/science.274.5292.1495>.
- NRC (National Research Council), 2007. The Scientific Context for Exploration of the Moon. The National Academies Press, Washington, DC. <https://doi.org/10.17226/11954>.
- Paige, D.A., et al., 2010. Diviner lunar radiometer observations of cold traps in the Moon's south polar region. *Science* 330, 479–482. <https://doi.org/10.1126/science.1187726>.
- Patterson, G.W., Stickle, A.M., Turner, F.S., Jensen, J.R., Bussey, D.B.J., Spudis, P., Espiritu, R.C., Schulze, R.C., Yocky, D.A., Wahl, D.E., Zimmerman, M., 2017. Bistatic radar observations of the moon using mini-RF on LRO and the Arecibo observatory. *Icarus* 283, 2–19.
- Pieters, C.M., Goswami, J.N., Clark, R.N., Annadurai, M., Boardman, J., Buratti, B., Combe, J.P., Dyar, M.D., Green, R., Head, J.W., Hibbitts, C., 2009. Character and spatial distribution of OH/H₂O on the surface of the Moon seen by M3 on Chandrayaan-1. *Science* 326 (5952), 568–572.
- Robbins, S.J., 2018. A new global database of lunar impact craters >1–2 km: 1. Crater locations and sizes, comparisons with published databases, and global analysis. *J. Geophys. Res.: Planets* 123. <https://doi.org/10.1029/2018JE005592>.
- Robinson, M.S., et al., 2010. Lunar reconnaissance orbiter camera (LROC) instrument overview. *Space Sci. Rev.* 150 (1–4), 81–124.
- Sanin, A.B., et al., 2016. Hydrogen distribution in the lunar polar regions. *Icarus* 283, 20–30. <https://doi.org/10.1016/j.icarus.2016.06.002>.
- Siegler, M., Paige, D., Williams, J.P., Bills, B., 2015. Evolution of lunar polar ice stability. *Icarus* 255, 78–87.
- Smith, D.E., et al., 2017. Summary of the results from the Lunar Orbiter Laser Altimeter after seven years in lunar orbit. *Icarus* 283, 70–91.
- Speyerer, E.J., Robinson, M.S., 2013. Persistently illuminated regions at the lunar poles: ideal sites for future exploration. *Icarus* 222, 122–136.
- Spudis, P.D., et al., 2016. Radar Data and Lunar Polar Volatiles. ISECG Lunar Polar Volatiles Virtual Workshop #1, Hosted by the NASA SSERVI.
- Spudis, P.D., Bussey, D.B.J., Baloga, S.M., Cahill, J.T.S., Glaze, L.S., Patterson, G.W., Raney, R.K., Thompson, T.W., Thomson, B.J., Ustinov, E.A., 2013. Evidence for water ice on the moon: results for anomalous polar craters from the LRO Mini-RF imaging radar. *J. Geophys. Res.* 118, 2016–2029.
- Spudis, D.B.J., Butler, B., Carter, L., Chakraborty, M., Gillis-Davis, J., Goswami, J., Heggy, E., et al., 2010a. Results of the Mini-SAR Imaging Radar, Chandrayaan-1 Mission to the Moon. LPSC 41st abstract #1224.
- Spudis, P.D., et al., 2010b. Mini-sar imaging radar and lunar polar ice. In: European Planetary Science Congress, 5, pp. EPSC2010–E2396.
- Spudis, P.D., et al., 2009. Mini-SAR: an imaging radar experiment for the Chandrayaan-1 mission to the Moon. *Curr. Sci.* 533–539.
- Spudis, P.D., Bussey, B., Plescia, J., Josset, J.L., Beauvivre, S., 2008. Geology of Shackleton crater and the South pole of the moon. *Geophys. Res. Lett.* 35 (14).
- Spudis, P.D., Gillis, J.J., Reisse, R.A., 1994. Ancient multiring basins on the Moon revealed by Clementine laser altimetry. *Science* 266 (5192), 1848–1851.
- Sunshine, J.M., Farnham, T.L., Feaga, L.M., Groussin, O., Merlin, F., Milliken, R.E., A'Hearn, M.F., 2009. Temporal and spatial variability of lunar hydration as observed by the Deep Impact spacecraft. *Science* 326 (5952), 565–568.
- Teodoro, L.F.A., Eke, V.R., Elphic, R.C., 2010. Spatial distribution of lunar polar hydrogen deposits after Kaguya (SELENE). *Geophys. Res. Lett.* 37, L12201.
- Watson, K., Murray, B., Brown, H., 1961. On the possible presence of ice on the Moon. *J. Geophys. Res.* 66, 1598–1600.

- Wilhelms, D.E., Howard, K.A., Wilshire, H.G., 1979. Geologic Map of the South Side of the Moon. Department of the Interior, US Geological Survey.
- Williams, J.P., Paige, D.A., Greenhagen, B.T., Sefton-Nash, E., 2017. The global surface temperatures of the moon as measured by the diviner lunar radiometer experiment. *Icarus* 283, 300–325.
- Xu, L., Zou, Y.L., Qing, L., 2019. Overview of China's lunar exploration program and scientific vision for future missions. In: Lunar and Planetary Science Conference, vol 50. LPI Contrib. No. 2132).
- Zhang, J.A., Paige, D.A., 2009. Cold-trapped organic compounds at the poles of the moon and Mercury: implications for origins. *Geophys. Res. Lett.* 36. <https://doi.org/10.1029/2009GL038614>.
- Zuber, M.T., Smith, D.E., 1997. Topography of the lunar south polar region: implications for the size and distribution of permanently shaded areas. *Geophys. Res. Lett.* 24, 2183–2186.